

Kinematics of young star clusters in the outer north-eastern region of the Small Magellanic Cloud

Andrés E. Piatti^{1,2,★}

¹ Instituto Interdisciplinario de Ciencias Básicas (ICB), CONICET-UNCuyo, Padre J. Contreras 1300, M5502JMA, Mendoza, Argentina;

² Consejo Nacional de Investigaciones Científicas y Técnicas (CONICET), Godoy Cruz 2290, C1425FQB, Buenos Aires, Argentina

Received / Accepted

ABSTRACT

It has been suggested since recent time that the magnitude of the interaction between galaxies could be measured from the level of kinematic disturbance of their outer regions with respect to the innermost ones. Here, I proved that the outer north-eastern region of the Small Magellanic Cloud (SMC), a relatively recent stellar structure with a tidal origin from the interaction with the Large Magellanic Cloud, is imprinted by a residual velocity pattern. I obtained from GEMINI GMOS spectra mean radial velocities of star clusters formed in situ, which added to derived mean proper motions and heliocentric distances, allowed to compute their 3D space velocity components. These space velocities differentiate from those that the clusters would have if they instead orderly rotated with the galaxy, i.e., their residual velocities are larger than the upper limit for an object pertaining to the SMC main body rotation disk. The level of kinematic disturbance depends on the SMC rotation disk adopted; galaxy rotation disks traced using relatively old objects are discouraged. The resulting kinematic disturbance arises in younger and older stellar populations, so that the epoch of close interaction between both Magellanic Clouds cannot be uncovered on the basis of the kinematics behavior of stellar populations populating the outer SMC regions.

Key words. techniques: spectroscopic – galaxies: individual: SMC – galaxies: star clusters

1. Introduction

In recent years, the tidal interaction between galaxies has become an issue of interest to understand their formation and evolution histories. One of the witnesses of such tidal interactions is the presence of an internal galactic kinematics pattern, which show increasing velocities dispersion towards the outermost galactic regions with respect to that in the innermost ones. For instance, Martínez-García et al. (2023) found that dwarf spheroidal satellites of the Milky Way present velocity gradients along the line-of-sight, indicating that the interaction with the Milky Way is causing them. To draw such a conclusion they combined proper motions from the *Gaia* Data Release 3 (DR3) (Gaia Collaboration et al. 2016; Babusiaux et al. 2023) and line-of-sight velocities from the literature to derive their 3D internal kinematics.

In this context, the outermost regions of the Small Magellanic Cloud (SMC), particularly those facing towards the Large Magellanic Cloud (LMC), are expected to have experienced the effects of the mutual tidal interaction more intensively than its stellar innermost component, which exhibit an orderly rotational motion (see, e.g. Niederhofer et al. 2018; Zivick et al. 2018; Di Teodoro et al. 2019, and references therein): the observed gaseous component not showing a evidence of ordered rotation (Murray et al. 2019; Rathore et al. 2025) though. However, the velocity gradient for the SMC has not been estimated yet (with the exception of one estimate by Zivick et al. (2021)), which is fundamental to contribute to our knowledge about the formation, evolution and interaction of these pair of galaxies.

Martínez-Delgado et al. (2019) studied the nature of a stellar structure (also called shell region) located 8° north-east from the SMC, and concluded that it formed in a recent star formation event, likely triggered by the interaction with the LMC. They also showed that the only 9 star clusters projected onto that structure are young, compatible with being part of it. Piatti (2022) used the Survey of the MAgellanic Stellar History (SMASH; Nidever et al. 2021) data base to derive ages and distances of these star clusters, and confirmed that they are young and span a heliocentric distance range ~ 3 times the depth of the SMC main body. Both, their youth and their large distance range along the same line-of-sight favor the tidal origin of this north-eastern stellar structure, making it suitable to investigate whether their kinematics differentiates from that of the rotating inner SMC main body.

If the kinematics of this outermost SMC region were affected by tidal effects, it should show a kinematics that departs from that of the rotating inner disk extrapolated toward this outermost region. Based on this, 3D velocities of star clusters aligned along the line-of-sight of the north-eastern stellar structure are important: 1) they add a valuable puzzle piece on the kinematics of the SMC at large distance from its center; 2) they help us to understand at what level the interaction of the SMC with the LMC affects its kinematics, and 3) they contribute to build a comprehensive map of the kinematic behavior of the SMC outermost regions, which is still a matter of work (see, e.g., Sloan Digital Sky Survey V: Kollmeier et al. 2019). Note that by kinematically studying these young clusters we improve our knowledge of the recent SMC formation, evolution and tidal interaction. Precisely, in this work I make use of spectroscopic and astrometric data to

* e-mail: andres.piatti@fcen.uncu.edu.ar

study the kinematics of star clusters in order to address this issue. Section 2 describes the collection and processing of the acquired spectroscopic data, Section 3 deals with the estimation of mean star clusters' radial velocities, while Section 4 is devoted to the analysis of the derived 3D star cluster velocities. Section 5 summarizes the main conclusions of this work.

2. Observational data

I used the GEMINI GMOS-S spectrograph, in multi-object mode, to get spectra with the grism B1200 (central $\lambda \sim 5000$ Å, spectral range 4200 - 5800 Å, dispersion 0.26 Å/pix) of stars in the fields of the SMC young star clusters HW 64, IC 1655, and IC 1660 (30-105 Myr; Piatti 2022), respectively. Stars were selected based on the membership probabilities of Piatti (2022), including stars only brighter than $g = 20$ mag. I obtained 3×510 sec exposures using a manufactured mask for each star cluster field through program GS-2025B-Q-101 (PI: Illesca). The collection of images included Cu-Ar arc lamps and flat-fields obtained before or after each individual science spectrum, as well as, nightly series of bias and observations of spectrophotometric standard stars. Figures 1 to 3 show the positions in the sky of the observed stars and their loci in the SMASH color-magnitude diagram (CMD).

The spectra images were reduced using the GEMINI task package¹ within the IRAF² environment. Science images were trimmed, corrected by overscan, bias, flat-field, and mosaiced. Then, the slits were properly cut so that the star spectra appeared centered on them. The mosaiced spectra images were wavelength calibrated, from which the individual star spectra were extracted, previously being background subtracted, and finally they were flux calibrated. I combined the three individual spectra per star in order to remove cosmic rays and increase the spectra S/N ratio. I employed the resulting spectra to measure radial velocity (RV) using the H β spectral line and the FXCOR task within IRAF. I applied the corresponding correction to attain heliocentric RVs. I derived RVs for most of the observed stars, whose values are listed in Table B.1, alongside the respective S/N ratio, the celestial equatorial coordinates and the observed SMASH g, i photometry.

3. Mean star clusters' radial velocity

In order to estimate the mean star clusters' RV, I took advantage of the fact that a cluster member not only has a RV similar to the mean value of the cluster, but also it is placed along the star cluster sequence in the CMD (see Figure 2 in Piatti 2022). These two parameters, the RV and the distance to the ridge line of the cluster sequence in the CMD, are characterized by showing over-densities of cluster members in that 2D plane. This means that any Gaussian mixture model can be applied to disentangle cluster members from field stars.

I computed the distance of each observed star to the theoretical isochrone of the respective cluster (see Figures 1 to 3) using the following expression:

$$d = \sqrt{((g - i) - (g - i)_{\text{iso}})^2 + k \times (g - g_{\text{iso}})^2}$$

where g and $(g - i)$ are the SMASH observed magnitudes and colors (see Table B.1) and g_{iso} and $(g - i)_{\text{iso}}$ are the theoretical

ones with the respective cluster reddening and distance modulus applied. I employed the cluster parameters (age, reddening, distance and metallicity) derived by Piatti (2022). The parameter k is a factor that put magnitudes and colors in the same scale. In this case, I adopted $k = 0.5$. In practice, for each $(g, g - i)$ pair I computed d using many points along the theoretical isochrone, and chose the g_{iso} and $(g - i)_{\text{iso}}$ values that minimized d . For the sake of the reader, I called d the scaled CMD distance. The uncertainties in d were computed by propagating the errors in g and $g - i$.

Figure 4 depicts the distribution of the measured stars in the RV versus scaled CMD distance plane. As can be seen, the observed sample of stars includes field stars spanning the whole ranges of RV and scaled CMD distance, and groups of stars that resemble those of cluster members. Field stars are seen placed along the cluster line-of-sight, mingled with cluster members, but having RVs different from that of cluster's stars and positions in the CMD out of the cluster sequences. Likewise, it is possible to find field stars with RVs similar to that of the cluster or close to the cluster's sequences in the CMD.

In order to detect any overdensity in the panels of Figure 4, which in turn provide the mean clusters' RVs, I used the Hierarchical Density-Based Spatial Clustering of Applications with Noise (HDBSCAN McInnes et al. 2017) Gaussian mixture model technique. The `min_cluster_size` parameter was varied between 3 and 8 dex in steps of 1 dex, until reached an optimum value where the number of selected stars remained constant. Since each observed cluster field contains only one star cluster, the respective RV versus scaled CMD distance plane should consequently harbor only one overdensity. For this reason, I considered `allow_single_cluster=True` during the execution of HDBSCAN. Figure 4 shows with magenta circles the stars found by HDBSCAN that exhibit clustering. I also highlight them from all the measures stars in Figures 1 to 3 with filled magenta symbols. As can be seen, all of them are within 0.10 mag from the corresponding CMD cluster sequence. From the selected clustered stars I estimated the mean clusters' RVs. Table 1 lists the reddening ($E(B - V)$), true distance modulus ($m - M_o$), age, and metallicity (Z) values for the three studied clusters, taken from Piatti (2022), together with the mean cluster RVs and the final number of confirmed cluster members identified from which the mean RVs are calculated. As far as I am aware, there are no previous mean star cluster RV estimates.

4. Analysis and discussion

With the aim of computing the 3D velocity components of HW 64, IC 1655, and IC 1660, I first derived the mean clusters' proper motions. For that purpose, I download from *Gaia* DR3 R.A. and Dec. coordinates, parallaxes (ϖ), proper motions in R.A. and Dec. (pmra , pmdec), with their associated uncertainties, and G , BP , and RP magnitudes of stars located inside circles with a radius of 4 arcmin from the centers of these three star clusters. I restricted the data to those with errors in both proper motions < 0.1 mas/yr, $\text{ruwe} < 1.4$ (Ripepi et al. 2019), and excluded confirmed nearby stars, i.e., $|\varpi| < 3\sigma(\varpi)$ (see Vasiliev 2018). Then, I built the clusters' CMDs and measured the scaled CMD distances d as in Section 3, using the *Gaia* theoretical isochrones (Bressan et al. 2012, PARSEC v1.2S). Finally, I fed HDBSCAN with the collected data for three variables: pmra , pmdec , and d , and identified the groups of stars satisfying cluster overdensity in that 3D phase space. The resulting mean clusters' proper motions are listed in Table 1, alongside with the number of stars used to compute them.

¹ <https://www.gemini.edu/observing/phase-iii/reducing-data/gemini-iraf-data-reduction-software>

² <https://iraf-community.github.io/>

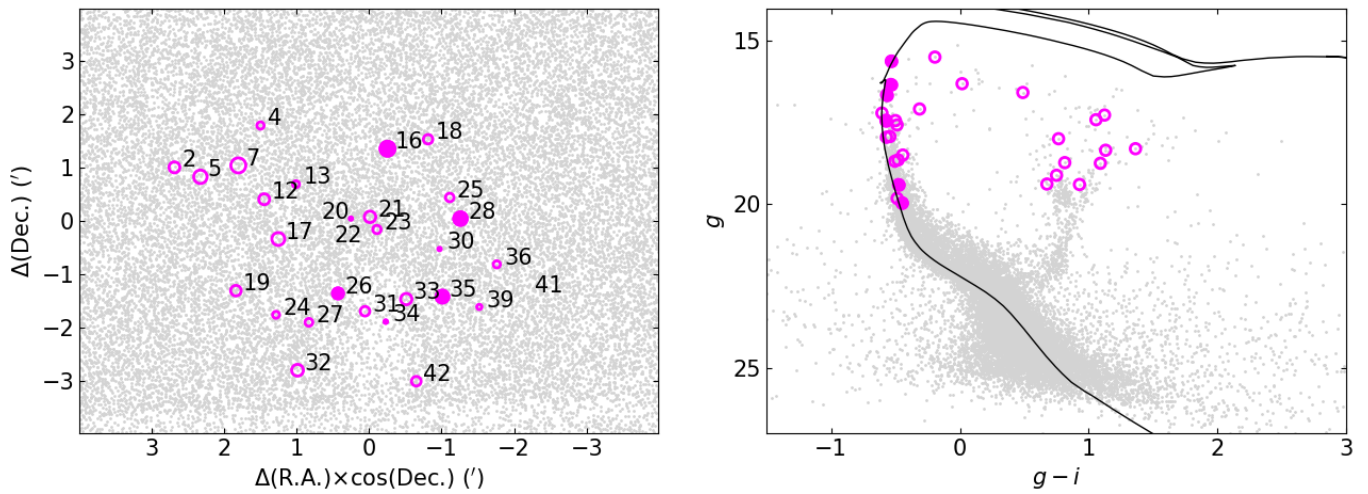


Fig. 1. *Left:* Sky map with stars observed by SMASH (gray points) and those observed in this work (large magenta circles) in the field of HW 64; symbol size being proportional to the g brightness of the star. Filled magenta circles represent cluster members (see details in Section 3). *Right:* SMASH color-magnitude diagram with the isochrone (Bressan et al. 2012, PARSEC v1.2S) corresponding to the distance, reddening, metallicity and age of the cluster (Piatti 2022), superimposed.

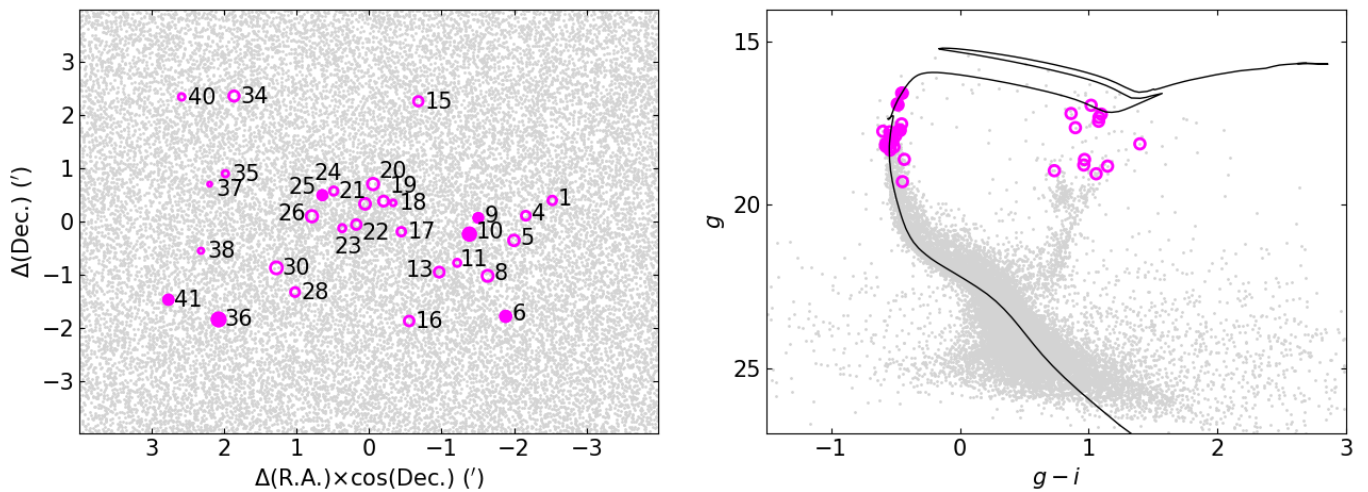


Fig. 2. Same as Figure 1 for IC 1655.

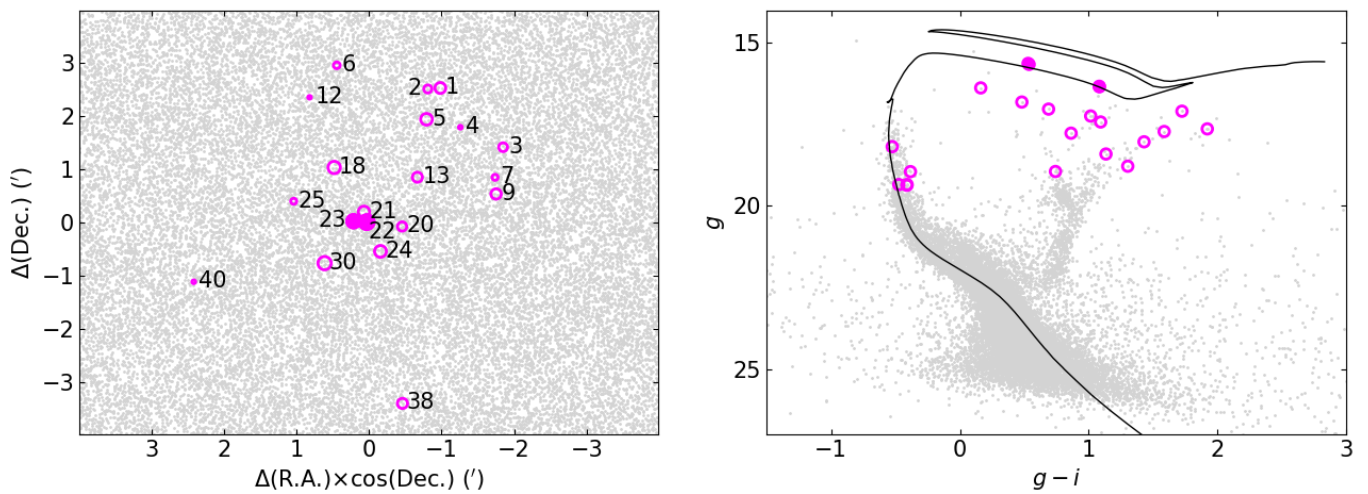
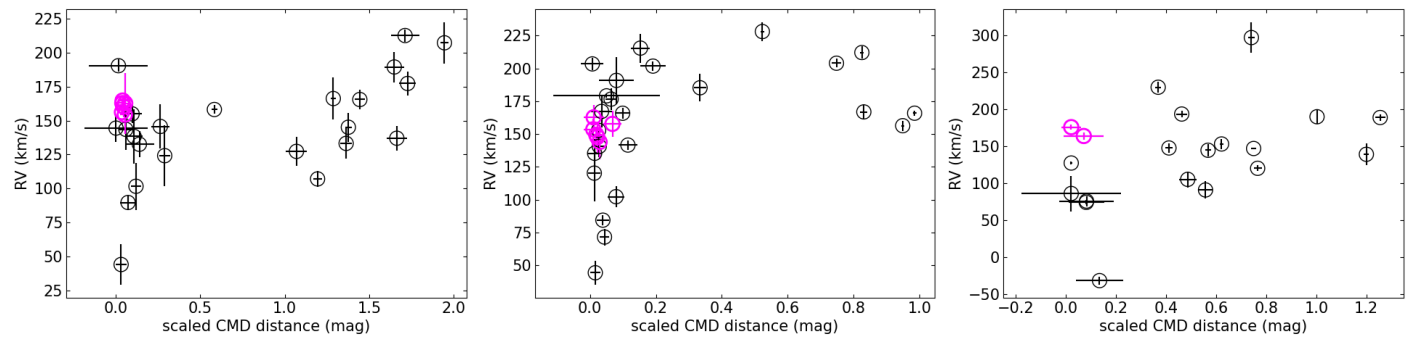


Fig. 3. Same as Figure 1 for IC 1660.

Table 1. Astrophysical properties of studied SMC star clusters.

Name	$E(B - V)$ (mag)	$m - M_o$ (mag)	$\log(\text{age}/\text{yr})$	Z (dex)	RV (km s^{-1})	N_{RV}	pmra (mas/yr)	pmdec (mas/yr)	N_{pm}
HW 64	0.142 ± 0.026	19.193 ± 0.083	7.468 ± 0.309	0.0064 ± 0.0029	160.24 ± 3.75	6	0.812 ± 0.032	-1.232 ± 0.028	6
IC 1655	0.129 ± 0.012	18.659 ± 0.039	8.054 ± 0.107	0.0037 ± 0.0015	152.52 ± 6.29	6	0.857 ± 0.098	-1.215 ± 0.065	6
IC 1660	0.139 ± 0.017	18.813 ± 0.055	7.909 ± 0.143	0.0054 ± 0.0023	170.20 ± 6.00	2	0.965 ± 0.112	-1.242 ± 0.054	6

**Fig. 4.** RV versus scaled CMD distance of stars in HW 64 (left panel), IC 1655 (middle panel), and IC 1660 (right panel), respectively. The magenta circles represent the selected clustered stars.

Piatti (2021b) used derived proper motions and radial velocities available in the literature of 25 SMC star clusters and the transformation Eqs. (9), (13), and (21) in van der Marel et al. (2002) to search for the kinematic model that best represents the motion of that cluster sample. He fit the R.A. and Dec., the heliocentric distance, the proper motion and the systemic velocity of the SMC center, in addition to the inclination, the position angle of the line-of-nodes, and the rotation velocity of the SMC disk. Table 2 lists the derived values. I here employed the transformation equations and the rotation model mentioned above to compute both, the 3D space velocity components of HW 64, IC 1655, and IC 1660, and those corresponding to points on the nominal SMC disk located at the clusters' distances from the SMC center. In doing that, I used the obtained mean clusters' RVs and proper motions and their heliocentric distances (D) estimated by Piatti (2022). The uncertainties were calculated using the measured errors in proper motion and radial velocity, and those from the model solution for the 3D movement of the SMC center, propagated through the transformation equations and added in quadrature.

When both velocity vectors are subtracted one with respect to the other and calculated the modulus of the resulting vector, an index called residual velocity (ΔV) is obtained (Piatti 2021a). ΔV is meant to measure the magnitude of kinematic disturbance of star clusters with respect to an orderly rotation galaxy disk. Figure 5, left panel, shows ΔV versus D for the three studied clusters represented with filled magenta circles ($D = 63.0, 53.9, 57.9$ kpc for HW 64, IC 1655, and IC 1660, respectively). I enlarged the sample of clusters genuinely belonging to the outer north-eastern region of the SMC by searching the literature for the necessary information to compute ΔV . Thus, I added HW 56 (3.09 Gyr Dias et al. 2021) and NGC 458 (0.14 Gyr Song et al. 2021), which are painted with filled red circles in Figure 5. Bearing in mind the SMC center and line-of-sight depth obtained by Piatti (2021b), which are represented by a solid and dashed vertical lines in Figure 5, respectively, and the boundary between bound and kinematically perturbed clusters ($\Delta V \sim 60 \text{ km s}^{-1}$; Piatti 2021a), the five star clusters pertaining to the outer north-eastern SMC structure would not seem to be perturbed by tidal

effects from the LMC. Their ΔV values are on average below $\sim 60 \text{ km s}^{-1}$.

However, ΔV depends on the SMC rotation disk adopted, so that a comprehensive analysis of the kinematic of the studied star clusters requires the consideration of different rotation disk models. Recently, Dhanush et al. (2025, and references therein) used *Gaia* DR3 data sets to derive kinematic parameters of different SMC stellar populations. Indeed, from young to old stellar population they found a change in the SMC disk inclination from $\sim 82^\circ$ down to $\sim 58^\circ$, and in the position angle of the line-of-nodes (LON) from $\sim 180^\circ$ up to $\sim 240^\circ$. Table 2 includes the values of the parameters adopted in this work for a representative young and old stellar population, making use of Dhanush et al. (2025)'s results. As for the SMC center proper motion, I adopted that of Niederhofer et al. (2021) for the optical center (de Vaucouleurs & Freeman 1972), which is in very good agreement with those from recent space-based data (Gaia Collaboration et al. 2018; Zivick et al. 2018; De Leo et al. 2020) and with Dhanush et al. (2025).

For these two representative SMC rotation disks, I computed ΔV and their uncertainties for the five studied star clusters in the outer north-eastern structure, and the resulting ΔV versus D relationships are depicted in Figure 5 (middle and right panels). As can be seen, the kinematics of the studied clusters with respect to the orderly motion of the young stellar population (Niederhofer et al. 2018; Zivick et al. 2018; Di Teodoro et al. 2019) would seem to reveal a kinematic gradient, in the sense that smaller the heliocentric distance (which means the closer to the LMC), the larger the ΔV value. This outcome suggests that tidal interactions with the LMC (the studied clusters are relatively young) could have imprinted certain agitation in their kinematics. This possibility would seem to be supported by the fact that the correlation of ΔV and D using the old star population kinematic model resulted to be similar to that from the cluster rotation model. Indeed, the 25 SMC clusters used by Piatti (2021b) to uncover their own kinematic model are intermediate-age to old globular clusters (age > 1 Gyr). In other words, the old star population rotation disk is based on the motions of perturbed stars located

in the outer SMC regions, and hence no readily visible gradient is seen in the left and right panels of Figure 5.

Hota et al. (2024) recently analyzed Ultra Violet Imaging Telescope (UVIT; Tandon et al. 2017) data and *Gaia* Early DR3 data of stars in the shell region in the north-eastern SMC. They split the star sample in three age groups: stars younger than 150 Myr; stars with ages between 150 and 300 Myr, and stars older than 300 Myr. They aimed to probe the kinematics of stars formed before and after the recent interaction between the LMC and the SMC ~ 250 Myr ago (Choi et al. 2022). They found no apparent kinematic distinction between the three age groups, concluding that they did not find any evidence of tidal perturbation or disruption in this part of the SMC. However, the lack of distinction between proper motions of stars belonging to the north-eastern shell with different ages is in agreement with the present findings. The stellar populations formed in a region affected by galactic tides, as is the case of the outer north-eastern region of the SMC, are kinematically perturbed by those tides. In the case of older stellar populations, they were perturbed by tides because they were there when the tidal interactions occurred; and for the younger populations, the kinematics disturbance comes from the gas out of which they formed, which were sealed by that kinematic agitation too. As shown in Figure 5 (right panel) young clusters and old star populations have similar kinematics in the outer north-eastern SMC shell ($\Delta V < 60 \text{ km s}^{-1}$), while the motions of these clusters visibly differentiate ($\Delta V > 60 \text{ km s}^{-1}$) when they are compared to those of an orderly rotation disk extrapolated to the outer SMC regions.

I finally computed the anisotropy (Bennet et al. 2022):

$$\beta = 1 - \frac{(\sigma V_r)^2 + (\sigma V_z)^2}{2(\sigma V_\phi)^2}, \quad (1)$$

where σV_r , σV_ϕ , and σV_z are the dispersion in the three cylindrical velocity components, respectively. To obtain these quantities, I first calculated the 3D velocity components of the five star clusters in cylindrical coordinates with their respective uncertainties. Then, I used a maximum likelihood approach by optimizing the probability \mathcal{L} that the five star clusters with velocities V_i ($V \equiv V_r, V_\phi, V_z$) and errors e_i are drawn from a population with mean $\langle V \rangle$ and dispersion σ (e.g., Pryor & Meylan 1993; Walker et al. 2006), as follows:

$$\mathcal{L} = \prod_{i=1}^N \left(2\pi(e_i^2 + \sigma^2) \right)^{-\frac{1}{2}} \exp\left(-\frac{(V_i - \langle V \rangle)^2}{2(e_i^2 + \sigma^2)} \right), \quad (2)$$

where the errors on the mean and dispersion were computed from the respective covariance matrices. As a result, I obtained σV_r , σV_ϕ , and σV_z with their corresponding uncertainties. Since the star clusters' velocities were computed using as reference a young and an old SMC kinematic disk (see Table 2), I finally got two different β values, namely: 0.06 ± 0.01 (young disk) and -6.30 ± 0.10 (old disk), where the mean and dispersion come from averaging a thousand values generated using Monte Carlo for $\sigma V_r = 12.2 \pm 0.1$, $\sigma V_\phi = 47.0 \pm 0.1$, and $\sigma V_z = 63.1 \pm 0.1$ (young disk), and $\sigma V_r = 13.9 \pm 0.5$, $\sigma V_\phi = 9.5 \pm 0.1$, and $\sigma V_z = 33.5 \pm 0.3$ (old disk), respectively. I note that a negative value implies a low azimuthal dispersion, i.e. ordered rotation, which indicates similarity between the observations and the kinematic model. The resulting β values reveal that the kinematics of the five star clusters in the outer north-eastern is more similar to that of the old SMC disk rather than to that of the young disk.

5. Conclusions

The strength of tidal effects caused by the interaction between galaxies should be reasonably measured by the level of kinematic disturbance of the outermost galactic regions with respect to that in the innermost ones. This work is aimed at confirming the above statement for the outer north-eastern region of the SMC, where is known that a recent stellar structure formed because of the interaction with the LMC (Martínez-Delgado et al. 2019; Piatti 2022; Dhanush et al. 2025). Since a number of young ($\lesssim 200$ Myr) star clusters also formed in this region during the interaction, I used a sample of them as kinematic tracers of that region and computed their residual velocities (ΔV).

To obtain ΔV values for HW 64, IC 1655, and IC 1660, three star clusters formed in the north-eastern shell, I performed Gemini GMOS-S multi-object observations, from which the mean star clusters' radial velocities were derived for the first time. The mean clusters' proper motions were also derived using *Gaia* DR3 data. The 3D space velocity components were calculated employing the derived mean proper motions and radial velocities, star clusters' heliocentric distance taken from the literature and the coordinates framework defined in van der Marel et al. (2002). The modulus of the vector difference between the cluster's velocity and that of a point in the SMC rotating disk at the cluster distance from the SMC center represents ΔV . The resulting ΔV values, to which I added those of two star clusters belonging to the north-eastern shell with the necessary information available (HW 56 and NGC 458), led me to conclude:

- When the SMC rotating disk fitted by Piatti (2021b) using star clusters older than ~ 1 Gyr is used as reference, the five studied star clusters would not seem to be kinematically perturbed. Their ΔV values are mostly $< 60 \text{ km s}^{-1}$, an upper limit found by Piatti (2021a) for the residual velocity of the SMC main body. The apparent lack of kinematic disturbance would seem to be the result of employing as reference a rotating disk that by itself is perturbed. A similar behavior is found if a rotating disk traced by old stellar populations is used.
- However, if an orderly rotating SMC disk fitted using young stellar populations mainly distributed in the innermost galaxy regions is used as reference (e.g., Dhanush et al. 2025), the star clusters exhibit a clear residual velocity gradient, in the sense that the farther a cluster from the SMC center (in this case also implies closer to the LMC), the larger its residual velocity (see, Figure A.1). This outcome is a clear evidence that galactic tides kinematically affects the outer galactic regions.
- The above results are in excellent agreement with the recent study by Dhanush et al. (2025), who performed the computation of different SMC rotation disk parameters employing a comprehensive sample of different stellar populations. Indeed, their results point to the existence of as many different rotation disk as galaxy stellar component are used, and highlight the prevailing orderly rotation motion in the innermost galaxy regions with respect to the outer ones, which are affected by tides.
- The results found in this work confirm that LMC tides kinematically affect the outer SMC regions, independently of the age of the stellar populations that populate those regions. This implies that the epoch of close interaction between both Magellanic Clouds is still active.

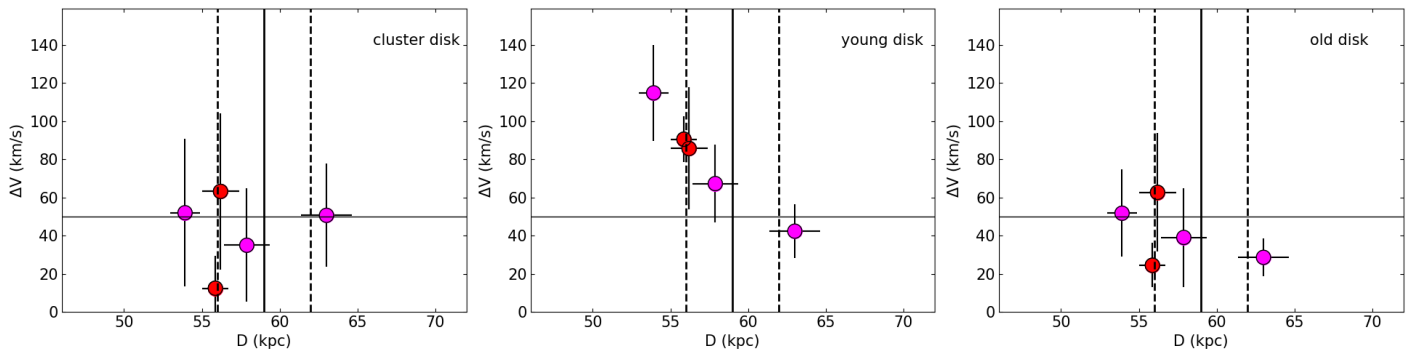


Fig. 5. ΔV versus heliocentric distance of young SMC clusters located in the north-eastern shell region. The solid and dashed vertical lines represent the galaxy center and its depth according to the cluster rotation disk (Piatti 2021b), while the horizontal line represents a boundary between bound and kinematically perturbed clusters. Magenta and red filled circles represent the present studied clusters and those taken from the literature, respectively. A kinematic gradient is present when compared to a young stellar model (middle panel), but absent in comparison to the old stellar and cluster models (right and left panels), respectively (see text for details).

Table 2. SMC rotation disk models.

Parameter	cluster disk	young disk (age < 50 Myr)	old disk (age > 2 Gyr)
SMC center R.A. (°):	13.30 ± 0.10	13.05	13.05
SMC center Dec. (°):	-72.85 ± 0.10	-72.83	-72.83
SMC center distance (kpc):	59.0 ± 1.5	62.44 ± 0.47	62.44 ± 0.47
SMC center pmra (mas/yr):	0.75 ± 0.10	-0.743 ± 0.027	-0.743 ± 0.027
SMC center pmdec (mas/yr):	-1.26 ± 0.05	-1.233 ± 0.012	-1.233 ± 0.012
SMC center systemic velocity (km s ⁻¹):	150.0 ± 2.0	145.6 ± 0.1	145.6 ± 0.1
SMC disk inclination (°):	70.0 ± 10.0	81.9 ± 0.7	58.4 ± 1.4
SMC disk position angle LON (°):	200.0 ± 30.0	185.7 ± 3.7	207.6 ± 2.3
SMC disk rotation velocity (km s ⁻¹):	25.0 ± 5.0	10.0 ± 5.0	10.0 ± 5.0

lanic Clouds cannot be uncovered from the kinematics of the outer SMC regions.

Acknowledgements. I thank the referee for the thorough reading of the manuscript and timely suggestions to improve it. Based on observations obtained at the international GEMINI Observatory, a program of NSF NOIRLab, which is managed by the Association of Universities for Research in Astronomy (AURA) under a cooperative agreement with the U.S. National Science Foundation on behalf of the GEMINI Observatory partnership: the U.S. National Science Foundation (United States), National Research Council (Canada), Agencia Nacional de Investigación y Desarrollo (Chile), Ministerio de Ciencia, Tecnología e Innovación (Argentina), Ministério da Ciência, Tecnologia, Inovações e Comunicações (Brazil), and Korea Astronomy and Space Science Institute (Republic of Korea). This work has made use of data from the European Space Agency (ESA) mission *Gaia* (<https://www.cosmos.esa.int/gaia>), processed by the *Gaia* Data Processing and Analysis Consortium (DPAC, <https://www.cosmos.esa.int/web/gaia/dpac/consortium>). Funding for the DPAC has been provided by national institutions, in particular the institutions participating in the *Gaia* Multilateral Agreement. Data for reproducing the figures and analysis in this work will be available upon request to the author.

Kollmeier, J., Anderson, S. F., Blanc, G. A., et al. 2019, in Bulletin of the American Astronomical Society, Vol. 51, 274
 Martínez-Delgado, D., Vivas, A. K., Grebel, E. K., et al. 2019, A&A, 631, A98
 Martínez-García, A. M., del Pino, A., & Aparicio, A. 2023, MNRAS, 518, 3083
 McInnes, L., Healy, J., & Astels, S. 2017, The Journal of Open Source Software, 2, 205
 Murray, C. E., Peek, J. E. G., Di Teodoro, E. M., et al. 2019, ApJ, 887, 267
 Nidever, D. L., Olsen, K., Choi, Y., et al. 2021, AJ, 161, 74
 Niederhofer, F., Cioni, M.-R. L., Rubel, S., et al. 2018, A&A, 613, L8
 Niederhofer, F., Cioni, M.-R. L., Rubel, S., et al. 2021, MNRAS, 502, 2859
 Piatti, A. E. 2021a, MNRAS, 508, 3748
 Piatti, A. E. 2021b, A&A, 650, A52
 Piatti, A. E. 2022, MNRAS, 509, 3462
 Pieres, A., Santiago, B. X., Drlica-Wagner, A., et al. 2017, MNRAS, 468, 1349
 Pryor, C. & Meylan, G. 1993, in Astronomical Society of the Pacific Conference Series, Vol. 50, Structure and Dynamics of Globular Clusters, ed. S. G. Djorgovski & G. Meylan, 357
 Rathore, H., Besla, G., van der Marel, R. P., & Kallivayalil, N. 2025, arXiv e-prints, arXiv:2512.06075
 Ripepi, V., Molinaro, R., Musella, I., et al. 2019, A&A, 625, A14
 Song, Y.-Y., Mateo, M., Bailey, J. I., et al. 2021, MNRAS, 504, 4160
 Tandon, S. N., Hutchings, J. B., Ghosh, S. K., et al. 2017, Journal of Astrophysics and Astronomy, 38, 28
 van der Marel, R. P., Alves, D. R., Hardy, E., & Suntzeff, N. B. 2002, AJ, 124, 2639
 Vasiliev, E. 2018, MNRAS, 481, L100
 Walker, M. G., Mateo, M., Olszewski, E. W., et al. 2006, AJ, 131, 2114
 Zivick, P., Kallivayalil, N., & van der Marel, R. P. 2021, ApJ, 910, 36
 Zivick, P., Kallivayalil, N., van der Marel, R. P., et al. 2018, ApJ, 864, 55

References

Babusiaux, C., Fabricius, C., Khanna, S., et al. 2023, A&A, 674, A32
 Bennet, P., Alfaro-Cuello, M., Pino, A. d., et al. 2022, ApJ, 935, 149
 Bressan, A., Marigo, P., Girardi, L., et al. 2012, MNRAS, 427, 127
 Choi, Y., Olsen, K. A. G., Besla, G., et al. 2022, ApJ, 927, 153
 De Leo, M., Carrera, R., Noël, N. E. D., et al. 2020, MNRAS, 495, 98
 de Vaucouleurs, G. & Freeman, K. C. 1972, Vistas in Astronomy, 14, 163
 Dhanush, S. R., Subramaniam, A., & Subramanian, S. 2025, ApJ, 980, 73
 Di Teodoro, E. M., McClure-Griffiths, N. M., Jameson, K. E., et al. 2019, MNRAS, 483, 392
 Dias, B., Angelo, M. S., Oliveira, R. A. P., et al. 2021, A&A, 647, L9
 Gaia Collaboration, Brown, A. G. A., Vallenari, A., et al. 2018, A&A, 616, A1
 Gaia Collaboration, Prusti, T., de Bruijne, J. H. J., et al. 2016, A&A, 595, A1
 Hota, S., Subramaniam, A., Dhanush, S. R., Cioni, M.-R. L., & Subramanian, S. 2024, MNRAS, 532, 322

Appendix A: Residual velocities

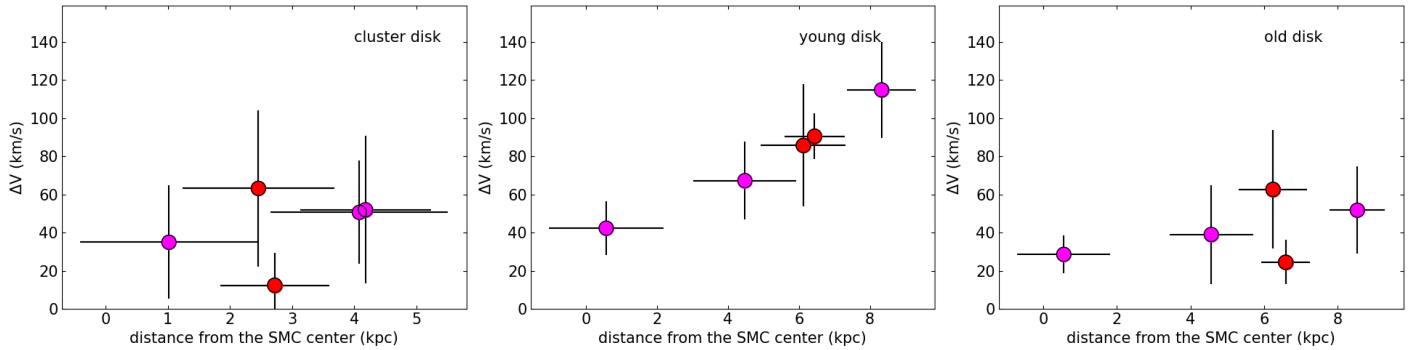


Fig. A.1. Same as Figure 5 using 3D distances from the SMC center, calculated using the models' parameters of Table 2.

Appendix B: Spectroscopic data

Table B.1.

Star	R.A. ($^{\circ}$)	Dec. ($^{\circ}$)	g (mag)	$g - i$ (mag)	S/N	RV (km s^{-1})
HW 64						
2	17.827	-71.322	17.41 \pm 0.01	1.05 \pm 0.06	19.6	137.05 \pm 8.91
4	17.766	-71.309	18.64 \pm 0.05	-0.47 \pm 0.05	20.8	154.98 \pm 6.69
5	17.809	-71.325	16.30 \pm 0.01	0.01 \pm 0.01	27.6	158.18 \pm 3.10
7	17.782	-71.322	15.49 \pm 0.04	-0.19 \pm 0.05	51.5	145.70 \pm 16.33
12	17.763	-71.332	17.43 \pm 0.04	-0.50 \pm 0.04	18.7	138.33 \pm 19.95
13	17.740	-71.328	18.74 \pm 0.01	1.09 \pm 0.05	13.0	189.48 \pm 11.17
16	17.675	-71.316	15.61 \pm 0.01	-0.53 \pm 0.01	54.3	156.21 \pm 1.58
17	17.753	-71.345	16.57 \pm 0.04	0.48 \pm 0.06	27.7	127.36 \pm 10.50
18	17.646	-71.314	17.99 \pm 0.02	0.76 \pm 0.03	14.8	133.24 \pm 11.11
19	17.784	-71.361	17.56 \pm 0.02	-0.48 \pm 0.02	14.2	101.68 \pm 17.38
20	17.701	-71.338	19.39 \pm 0.02	0.92 \pm 0.02	5.0	165.53 \pm 7.32
21	17.687	-71.338	17.20 \pm 0.14	-0.60 \pm 0.20	24.3	144.49 \pm 10.01
22	17.692	-71.341	19.81 \pm 0.12	-0.48 \pm 0.18	23.7	190.41 \pm 4.53
23	17.682	-71.342	18.34 \pm 0.07	1.13 \pm 0.08	13.2	212.62 \pm 4.57
24	17.755	-71.368	18.72 \pm 0.01	0.81 \pm 0.02	11.1	145.13 \pm 10.71
25	17.630	-71.332	18.29 \pm 0.01	1.36 \pm 0.02	14.6	207.26 \pm 15.25
26	17.710	-71.362	17.42 \pm 0.02	-0.57 \pm 0.02	27.1	164.77 \pm 3.41
27	17.731	-71.371	18.49 \pm 0.08	-0.44 \pm 0.08	10.7	132.59 \pm 9.69
28	17.622	-71.338	16.33 \pm 0.04	-0.53 \pm 0.04	49.2	160.44 \pm 7.77
30	17.637	-71.348	19.37 \pm 0.02	0.67 \pm 0.02	6.8	107.08 \pm 5.69
31	17.691	-71.367	17.94 \pm 0.02	-0.57 \pm 0.03	21.8	44.09 \pm 14.84
32	17.740	-71.386	17.08 \pm 0.02	-0.31 \pm 0.03	28.8	124.18 \pm 22.67
33	17.661	-71.364	17.26 \pm 0.03	1.12 \pm 0.04	22.2	177.35 \pm 8.66
34	17.676	-71.371	19.39 \pm 0.02	-0.47 \pm 0.02	6.5	154.39 \pm 3.29
35	17.635	-71.363	16.64 \pm 0.01	-0.56 \pm 0.02	64.2	162.87 \pm 1.80
36	17.596	-71.353	18.68 \pm 0.03	-0.50 \pm 0.04	11.6	89.73 \pm 4.91
39	17.609	-71.366	19.11 \pm 0.01	0.75 \pm 0.01	8.9	166.25 \pm 15.58
41	17.574	-71.361	19.95 \pm 0.01	-0.44 \pm 0.02	14.0	162.79 \pm 22.36
42	17.654	-71.389	17.92 \pm 0.02	-0.54 \pm 0.04	15.8	143.56 \pm 15.28
IC 1655						
1	17.841	-71.323	18.21 \pm 0.01	-0.54 \pm 0.01	25.9	45.16 \pm 9.09
4	17.860	-71.328	18.12 \pm 0.01	-0.57 \pm 0.01	20.2	141.42 \pm 8.21
5	17.868	-71.336	17.51 \pm 0.02	-0.45 \pm 0.02	26.3	103.06 \pm 8.26
6	17.874	-71.360	17.69 \pm 0.02	-0.46 \pm 0.02	16.6	158.46 \pm 9.97
8	17.887	-71.347	17.31 \pm 0.01	1.08 \pm 0.03	21.8	166.57 \pm 4.04
9	17.894	-71.329	18.19 \pm 0.01	-0.57 \pm 0.01	18.6	144.72 \pm 13.26
10	17.900	-71.334	16.90 \pm 0.02	-0.48 \pm 0.03	36.3	163.45 \pm 9.15

Table B.1.

Star	R.A. ($^{\circ}$)	Dec. ($^{\circ}$)	g (mag)	$g - i$ (mag)	S/N	RV (km s $^{-1}$)
IC 1660						
11	17.911	-71.343	18.60 \pm 0.01	-0.43 \pm 0.02	19.7	142.34 \pm 3.53
13	17.922	-71.346	17.75 \pm 0.02	-0.54 \pm 0.02	25.1	136.07 \pm 10.60
15	17.937	-71.292	17.94 \pm 0.03	-0.52 \pm 0.03	18.2	167.92 \pm 12.41
16	17.944	-71.361	17.87 \pm 0.01	-0.54 \pm 0.02	21.1	120.98 \pm 21.75
17	17.949	-71.333	18.22 \pm 0.01	-0.51 \pm 0.01	21.0	85.19 \pm 3.66
18	17.955	-71.324	18.94 \pm 0.01	0.73 \pm 0.01	12.7	166.60 \pm 2.10
19	17.962	-71.323	17.74 \pm 0.01	-0.59 \pm 0.01	28.8	177.32 \pm 8.04
20	17.969	-71.318	17.21 \pm 0.01	1.09 \pm 0.22	23.8	179.81 \pm 1.28
21	17.975	-71.324	17.43 \pm 0.01	1.07 \pm 0.07	20.1	216.15 \pm 11.00
22	17.981	-71.331	17.87 \pm 0.01	-0.49 \pm 0.01	18.1	72.33 \pm 6.26
23	17.991	-71.332	18.60 \pm 0.01	0.96 \pm 0.01	16.6	204.65 \pm 3.34
24	17.998	-71.320	18.31 \pm 0.03	-0.54 \pm 0.03	15.1	204.12 \pm 4.56
25	18.006	-71.322	18.08 \pm 0.01	-0.54 \pm 0.01	20.4	150.19 \pm 5.37
26	18.013	-71.328	17.19 \pm 0.02	0.86 \pm 0.05	21.2	202.44 \pm 3.78
28	18.026	-71.352	18.12 \pm 0.01	1.39 \pm 0.01	13.3	228.74 \pm 7.21
30	18.039	-71.344	16.94 \pm 0.01	1.01 \pm 0.01	25.2	153.60 \pm 2.37
34	18.069	-71.290	17.63 \pm 0.01	0.89 \pm 0.02	19.2	185.97 \pm 10.59
35	18.075	-71.315	18.80 \pm 0.01	1.14 \pm 0.01	9.5	212.77 \pm 4.66
36	18.080	-71.360	16.57 \pm 0.02	-0.45 \pm 0.03	40.8	154.33 \pm 7.99
37	18.087	-71.318	19.28 \pm 0.05	-0.44 \pm 0.05	8.1	191.58 \pm 17.89
38	18.093	-71.339	19.04 \pm 0.01	1.05 \pm 0.01	17.0	157.08 \pm 3.80
40	18.106	-71.291	18.77 \pm 0.01	0.96 \pm 0.01	9.7	167.59 \pm 5.83
41	18.116	-71.354	18.02 \pm 0.01	-0.52 \pm 0.01	24.5	148.43 \pm 11.85
1	18.104	-71.719	17.42 \pm 0.01	1.09 \pm 0.03	17.6	195.45 \pm 4.10
2	18.113	-71.719	18.40 \pm 0.01	1.13 \pm 0.01	9.7	191.78 \pm 9.69
3	18.058	-71.738	18.18 \pm 0.01	-0.52 \pm 0.01	10.8	129.19 \pm 1.86
4	18.089	-71.731	19.34 \pm 0.04	-0.41 \pm 0.11	5.1	77.76 \pm 6.92
5	18.114	-71.729	17.09 \pm 0.01	1.72 \pm 0.01	17.0	231.68 \pm 7.70
6	18.179	-71.712	18.78 \pm 0.01	1.30 \pm 0.01	29.5	141.02 \pm 14.88
7	18.064	-71.747	18.94 \pm 0.01	0.74 \pm 0.02	25.4	190.74 \pm 4.14
9	18.063	-71.752	17.63 \pm 0.01	1.92 \pm 0.01	15.3	298.81 \pm 20.94
12	18.199	-71.722	19.36 \pm 0.07	-0.41 \pm 0.07	16.7	75.90 \pm 2.96
13	18.121	-71.747	17.76 \pm 0.01	0.86 \pm 0.01	14.6	148.85 \pm 1.37
18	18.182	-71.744	16.81 \pm 0.01	0.48 \pm 0.01	30.5	146.47 \pm 8.29
20	18.132	-71.763	18.03 \pm 0.01	1.43 \pm 0.04	11.9	122.08 \pm 3.80
21	18.160	-71.758	17.24 \pm 0.01	1.01 \pm 0.01	22.4	149.55 \pm 6.10
22	18.158	-71.761	15.63 \pm 0.07	0.53 \pm 0.18	47.3	165.72 \pm 4.77
23	18.168	-71.761	16.33 \pm 0.01	1.08 \pm 0.09	25.4	177.73 \pm 3.39
24	18.148	-71.770	17.03 \pm 0.01	0.68 \pm 0.04	20.3	92.80 \pm 11.74
25	18.211	-71.755	18.94 \pm 0.09	-0.38 \pm 0.09	21.4	-29.76 \pm 5.50
30	18.189	-71.774	16.38 \pm 0.01	0.16 \pm 0.07	43.5	107.13 \pm 10.74
38	18.132	-71.818	17.71 \pm 0.01	1.58 \pm 0.01	23.5	154.97 \pm 6.76
40	18.285	-71.780	19.34 \pm 0.13	-0.47 \pm 0.21	18.7	88.01 \pm 23.89